AGU PUBLICATIONS

Geophysical Research Letters

RESEARCH LETTER
10.1002/2016GL071829

Key Points:
- Atlantic Nino mode is much more symmetric than Pacific El Nino–Southern Oscillation
- Equatorial Atlantic cold events are mirror images of warm events
- Bjerknes feedback terms are more linear in the Atlantic than in the Pacific

Supporting Information:
- Supporting Information S1

Correspondence to:
J. F. Lübbecke,
jluebbecke@geomar.de

Citation:
Lübbecke, J. F., and M. J. McPhaden (2017), Symmetry of the Atlantic Niño mode, *Geophys. Res. Lett.*, *44*, 965–973, doi:10.1002/2016GL071829.

Received 4 NOV 2016
Accepted 30 DEC 2016
Accepted article online 4 JAN 2017
Published online 21 JAN 2017

Symmetry of the Atlantic Niño mode

Joke F. Lübbecke[1] and Michael J. McPhaden[2]

[1]GEOMAR Helmholtz Centre for Ocean Research Kiel, Kiel, Germany, [2]NOAA PMEL, Seattle, Washington, USA

Abstract El Niño–Southern Oscillation (ENSO) in the Pacific is asymmetric for warm and cold events with respect to amplitude, spatial patterns, and temporal evolution. Here the symmetry of the Atlantic Niño mode, which many previous studies have argued is governed by atmosphere-ocean dynamics similar to those of ENSO, is investigated using two different ocean reanalysis products. Calculation of Bjerknes feedback terms for the Pacific reveals a pronounced asymmetry between warm and cold events, though unlike most previous studies, the largest asymmetry is found in the relationship between eastern Pacific thermocline depth and sea surface temperature anomalies. For the Atlantic, cold events are effectively mirror images of warm events with Bjerknes feedbacks of similar strength. The analysis supports not only the conclusion that Atlantic Niños are more symmetric than ENSO but also the hypothesis itself that the Bjerknes feedback is operative in the Atlantic given the strength of the relationship between the key variables involved.

1. Introduction

In both the eastern equatorial Pacific and Atlantic Ocean, pronounced anomalies in sea surface temperatures (SSTs) occur on interannual time scales. These anomalies are an expression of the El Niño–Southern Oscillation (ENSO) and the Atlantic Niño mode, respectively [e.g., *Chang et al.*, 2006]. While differences in the character of these two phenomena exist, as, for example, in the strength and seasonality of the SST anomalies [e.g., *Keenlyside and Latif*, 2007; *Burls et al.*, 2012], they are both related to equatorial wind stress and equatorial thermocline variations via the Bjerknes feedback [*Bjerknes*, 1969]. Understanding the Atlantic Niño mode variability is of socioeconomic importance as SST anomalies in the eastern equatorial Atlantic are related to precipitation over Northeast Brazil [*Ruiz-Barradas et al.*, 2000] and the onset of the West African monsoon [*Brandt et al.*, 2011a]. The equatorial Atlantic also affects the equatorial Pacific Ocean [e.g., *Rodriguez-Fonseca et al.*, 2009], so that accounting for equatorial Atlantic SST variability may improve the prediction of El Niño events [*Keenlyside et al.*, 2013].

The Pacific ENSO mode is not symmetric for warm (El Niño) and cold (La Niña) events in terms of development, strength, duration, and location of maximum anomalies [e.g., *Larkin and Harrison*, 2002; *Shinoda et al.*, 2011]. For example, El Niños tend to be stronger than La Niñas, are of shorter duration, and have their maximum SST anomaly located farther to the east. This asymmetry has been explained by nonlinearities in the components of the Bjerknes feedback and the atmospheric heat flux damping. *Hoerling et al.* [1997] argued that the response to tropical Pacific SST forcing is inherently nonlinear due to the nonlinearity in the thermodynamic control on deep convection. *Meinen and McPhaden* [2000] reported that positive anomalies in warm water volume (WWV) are associated with larger SST anomalies than negative WWV anomalies of comparable size. *Su et al.* [2010] found that nonlinear zonal and meridional temperature advection by ocean currents was crucial for El Niño and La Niña amplitude asymmetry. *Kang and Kug* [2002] showed that wind stress anomalies related to La Niña are shifted westward compared to those related to El Niño. Based on those results, *Frauen and Dommenget* [2010] and *Dommenget et al.* [2012] suggested that the ENSO skewness in amplitude, spatial pattern, and time evolution is related to the nonlinear response of zonal winds to SST anomalies. These authors also found that a quadratic regression fit between Nino3 SST and central Pacific zonal wind stress anomalies was more suitable for large SST anomalies. *Choi et al.* [2013] also stressed the importance of enhanced wind stress sensitivity to SST changes during El Niño as contributing to the asymmetry of ENSO in a study based on a conceptual delayed oscillator model. Using the Bjerknes stability index defined by *Jin et al.* [2006], *Im et al.* [2015] recently pointed out that the dynamical ocean response per unit anomalous zonal wind stress is also larger during El Niño compared to La Niña phases. To summarize, nonlinearities in both the atmospheric and oceanic mechanisms that give rise to El Niño and La Niña events have been argued to cause the pronounced asymmetry between the cold and warm phases of ENSO.

A variety of processes have been suggested to contribute to the generation of Atlantic Niño events. Several studies have demonstrated that even though weaker than in the Pacific, the Bjerknes feedback is active in the equatorial Atlantic [e.g., *Zebiak*, 1993; *Keenlyside and Latif*, 2007; *Lübbecke and McPhaden*, 2013; *Deppenmeier et al.*, 2016]. Other mechanisms that have been discussed involve meridional advection of temperature anomalies [*Richter et al.*, 2013], forcing from equatorial deep jets [*Brandt et al.*, 2011b], and heat flux forcing [*Nnamchi et al.*, 2015]. Despite the differences that exist between ENSO and the Atlantic Niño mode, our working hypothesis, based on several studies like those cited above, is that the Bjerknes feedback plays a central role in the equatorial Atlantic. Using the Bjerknes feedback as a diagnostic framework, our purpose is then to address the question of whether the Atlantic Niño mode shows the same asymmetry between warm and cold events as ENSO.

2. Data and Methods

We use monthly fields of ocean temperature, wind stress, and heat flux from the Ocean Reanalysis System 4 (ORA-S4) of the European Centre for Medium-Range Weather Forecasts (ECMWF) [*Balmaseda et al.*, 2013] for the time period 1958 to 2009. It is based on version 3.0 of the Nucleus for European Modeling of the Ocean (NEMO) model at a horizontal resolution of 1°, forced with ERA-40 (1958 to 1988) and ERA-Interim (1989 to 2009) surface winds and heat fluxes. For comparison, we also use the "historical" simulation from the Simple Ocean Data Assimilation (SODA) reanalysis product (SODAv2.2.4) [*Carton and Giese*, 2008] for the same time period as for ORA-S4, namely, 1958 to 2009. SODAv2.2.4 is forced with 20CRv2 surface winds [*Compo*, 2011] and has 40 vertical levels and a horizontal resolution of 0.25°. We have calculated interannual anomalies by subtracting a mean seasonal cycle as well as the linear trend of the time series. To characterize variability in the eastern portions of the basins, we average variables over the Atl3 (20°W to 0°E, 3°S to 3°N) and Nino3 (150°W to 90°W, 5°S to 5°N) regions, respectively; to characterize variability to the west of these index regions, we use averages in the WAtl (40°W to 20°W, 3°S to 3°N) and Nino4 (160°E to 150°W, 5°S to 5°N) areas.

Following the work of *Larkin and Harrison* [2002] for the equatorial Pacific, we first compare composites of Atlantic Niño and Niña phases. Atlantic Niño and Niña years are defined as years in which detrended interannual SST anomalies averaged over the Atl3 region exceed the standard deviation of the time series for at least 2 months between May and September. These months are chosen because Atlantic Niño events are known to peak in boreal summer [e.g., *Carton and Huang*, 1994; *Keenlyside and Latif*, 2007]. Using the time period 1958 to 2009, we find 14 warm and 15 cold events.

The individual components of the Bjerknes feedback are then calculated separately for the Atlantic Niño mode warm and cold phases via linear least squares regression and compared to the corresponding results from the Pacific. We determine error bounds for 95% confidence levels of the regression slopes by calculating the standard errors of the slopes and then multiplying them by critical values according to a *t*-distribution.

3. Results

3.1. Composites of Atlantic Warm and Cold Events

Composites of interannual anomalies of SST, the depth of the 20°C isotherm as a measure of thermocline depth (z20), and wind stress from ORA-S4 are shown for Atlantic warm and cold events separately (Figure 1). The patterns are remarkably similar; i.e., the timing of the events is almost identical, and the amplitude of the cold events is essentially equal and opposite to that of warm events which have previously been described, for example, by *Carton and Huang* [1994]. An SST anomaly develops at the Angolan coast already in April, in agreement with the findings of *Hu and Huang* [2007] and *Lübbecke et al.* [2010]. It reaches the cold tongue region in May and is most pronounced in June and July with an amplitude of about 1°C before starting to decay in August. By September, only weak SST anomalies remain. Consistent with the warming (cooling), the thermocline deepens (shoals) in the east. As expected from the Bjerknes feedback mechanism, the southeasterly trades weaken (strengthen) in the months prior to the warming (cooling). SST composites from observational data sets, such as COBE SST2 and ERSSTv3, agree very well with the results from the reanalysis product (Figure S1 in the supporting information).

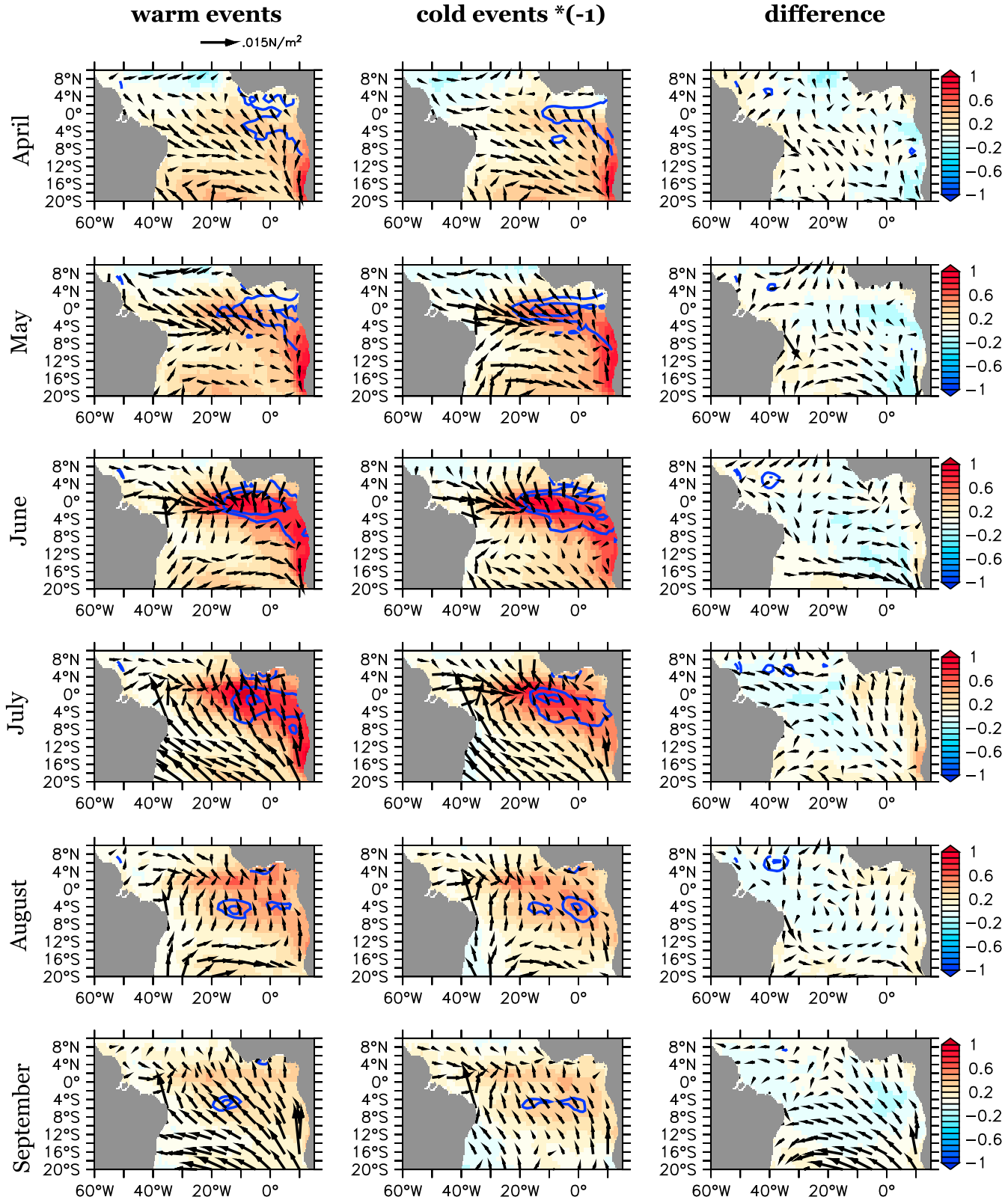

Figure 1. Composite anomalies around the climatological mean for April to September SST (color shading), wind stress (vectors), and thermocline depth (blue 3 m and 5 m contour lines for 10°S to 10°N) for (left column) years with Atlantic Niño events, (middle column) years with Atlantic Niña events (inverted), and (right column) their difference for the time period 1958 to 2009 from ORA-S4. A version of this figure showing only values significant at the 95% level is shown in the supporting information (Figure S2).

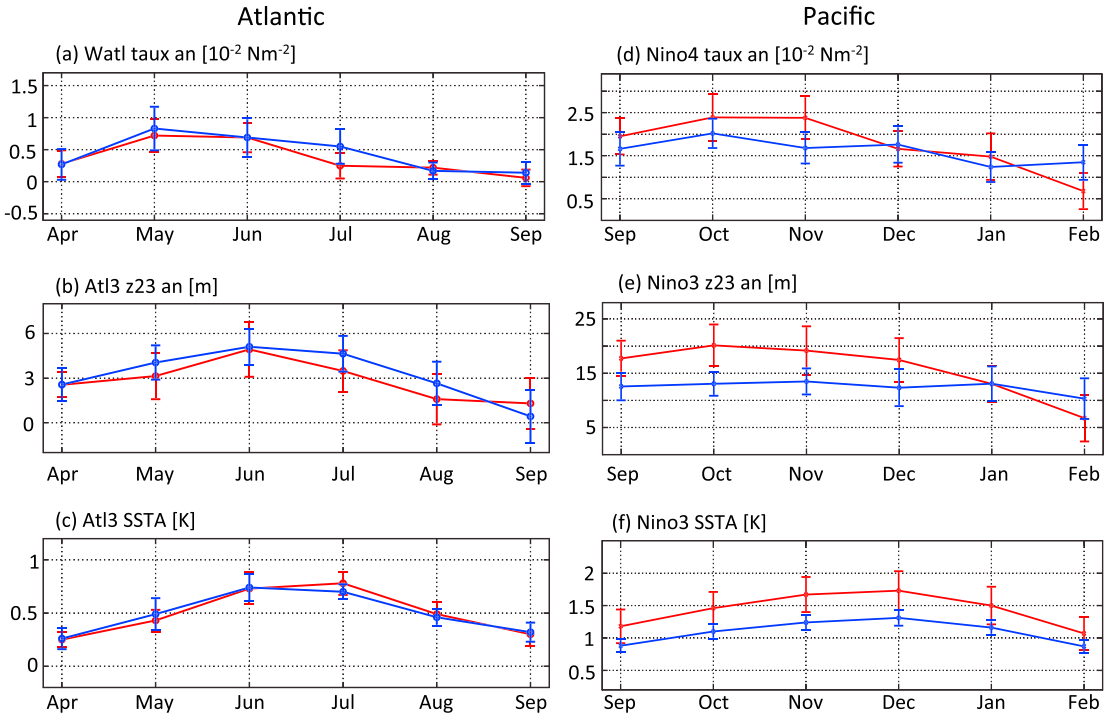

Figure 2. Evolution of (a) WAtl and (d) Nino4 zonal wind stress anomalies, (b) Atl3 and (e) Nino3 thermocline depth (defined as the depth of the 23°C isotherm) anomalies, and (c) Atl3 and (f) Nino3 SST anomalies for warm (red) and cold (blue) event years from ORA-S4 for the time period 1958 to 2009. The values for the cold events have been inverted for better comparison. Error bars denote one standard error.

The impression that Atlantic Niño and Niña events are essentially mirror images of one another is confirmed by the difference between the warm and (inverted) cold anomalies. Apart from a stronger warm signal at the Angolan coast in July and stronger southeasterly trade wind anomalies in September, the differences are small (Figure 1, right column). We actually find that except for an SST signal in a small area at the Angolan coast in July, none of the differences is significant at the 95% level (Figure S2). While this difference in the Benguela region is interesting in light of the connection between warm events off Angola and in the equatorial Atlantic [*Lübbecke et al.*, 2010], it appears to be only minor in comparison to the differences in both amplitude and position of El Niño and La Niña SST anomalies [e.g., *Im et al.*, 2015]. In contrast, there is clearly no such systematic difference between Atlantic Niño and Niña events, with respect to either the strength or the location of the anomalies.

To further illustrate the symmetry in the time evolution of the events, Figure 2 shows composites of WAtl zonal wind stress anomalies, Atl3 thermocline depth anomalies, and SST anomalies as a function of calendar month from April to September for Atlantic Niño and Niña years. These time series support the conclusion drawn from the composite maps (Figure 1) that cold and warm events develop analogous to each other and are associated with anomalies of similar amplitude. Eastern basin SST anomalies reach their maximum in June and July and then start to decay in August. Western basin zonal wind stress anomalies are strongest in May, followed by eastern basin thermocline anomalies that peak in June, consistent with equatorial Kelvin wave signal propagation from west to east (Figures 2a–2c). In contrast, in the equatorial Pacific, the amplitudes of the eastern basin thermocline depth and SST anomalies are clearly larger for El Niño than for La Niña (Figures 2e and 2f).

The rather symmetric behavior in terms of amplitude is further supported by the skewness of Atl3 SST anomalies, which is basically zero in ORA-S4 as well as in several observational SST data sets (Table S1). In contrast, the skewness for Nino3 SST anomalies is clearly positive (between 0.80 and 0.95) in all of those data sets, illustrating the larger amplitudes of El Niño vis-à-vis La Niña events. These results indicate that the Atlantic Niño mode is much more symmetric than ENSO in the Pacific. To further elucidate why this is the case with respect to amplitude, we examine the individual Bjerknes feedback terms for both the Atlantic and Pacific in the next section.

3.2. Bjerknes Feedback Terms for Warm and Cold Events

The Bjerknes feedback consists of three components: (i) SST anomalies in the eastern part of the basin forcing wind stress anomalies to the west, (ii) wind stress anomalies in the west leading to anomalies in thermocline depth that propagate eastward as Kelvin waves, and (iii) eastern equatorial thermocline depth anomalies inducing local SST anomalies, thereby amplifying the initial anomalies and closing the feedback loop. In Figure 3, the individual components of the Bjerknes feedback are shown for the equatorial Atlantic and Pacific. The slope of the linear regression is calculated separately for warm and cold SST anomalies. As ENSO tends to peak in boreal winter and the Atlantic Niño is phase locked to boreal summer, anomalies are considered for the individual calendar months that show the highest correspondence within the winter (Pacific) and summer (Atlantic) seasons as illustrated by the seasonally stratified cross correlation between the variables (Figures S3 and S4). For the Pacific we used a combination of 2 months each in order to reduce the influence of intraseasonal variability related to the Madden-Julian oscillation (MJO). While the correlations and the amplitudes of the feedbacks are generally lower and more uncertain when all calendar months are considered, the main results remain unchanged.

The first feedback component, i.e., the western basin wind response to eastern basin SST anomalies, represents a fast atmospheric response. Maximum correlations are consequently found for zero lag for both the tropical Atlantic and Pacific Ocean (Figures S3a and S4a). In the Atlantic, the strongest relationship occurs in May in ORA-S4 (Figure S3a). The linear regression between May Atl3 SST anomalies and May WAtl zonal wind stress anomalies is shown in Figure 3a. The two time series are well correlated at 0.75 for the warm and 0.86 for the cold SST anomalies. The slope—as a measure of the feedback strength—is very similar for positive and negative SST anomalies, being $1.85 \pm 0.46 \times 10^{-2}\,\mathrm{N\,m^{-2}\,K^{-1}}$ and $1.96 \pm 0.34 \times 10^{-2}\,\mathrm{N\,m^{-2}\,K^{-1}}$, respectively. These values are much higher than the ones found by *Lübbecke and McPhaden* [2013] for all calendar months, reflecting the seasonal dependence of the Atlantic Niño mode. Interestingly, the slope of the linear regression between October–November Nino3 SST and October–November Nino4 zonal wind stress anomalies—the months that are most highly correlated in the Pacific (Figure S4a)—is found to be slightly smaller than for the Atlantic but very similar for positive and negative SST anomalies as well ($1.48 \pm 0.17 \times 10^{-2}\,\mathrm{N\,m^{-2}\,K^{-1}}$ and $1.64 \pm 0.31 \times 10^{-2}\,\mathrm{N\,m^{-2}\,K^{-1}}$, respectively), despite the fact that warm SST anomalies tend to be much larger than cold anomalies (Figure 3b). This symmetry in the wind stress response to SST anomalies is consistent with the results of *Im et al.* [2015] but appears to disagree with studies highlighting the importance of the nonlinearity in this feedback for ENSO. Part of this discrepancy stems from the fact that we average the zonal wind response across the entire Nino4 region so that differences in the spatial patterns, i.e., a more westward shift for La Niña compared to El Niño as reported by *Kang and Kug* [2002], are not apparent. Calculating the regression pattern of Nino3 SSTA against zonal wind anomalies from ORA-S4 for all calendar months, we do find such a westward shift, albeit not as pronounced as reported in other studies. However, using only October SST and zonal wind anomalies, there is no clear westward shift (not shown) implying that there is also a difference due to the fact that we focus on individual calendar months that show the highest correlation. Calculating the feedback terms based on all calendar months does, however, not lead to a significant asymmetry. Another difference compared to previous studies is that we only calculate a linear regression in contrast to a higher-order fit as considered by *Frauen and Dommenget* [2010] and *Dommenget et al.* [2012]. Also, some of the previous studies based their analysis on different time periods.

In the second feedback component, zonal wind stress anomalies in the western equatorial basin drive thermocline slope variations along the equator, here calculated as the difference between the depth of the thermocline in the eastern and western regions. This response is accomplished by the eastward propagation of wind-forced equatorial waves. The highest correlation thus occurs at a lag of about 1 month (Figures S3b and S4b). In the Atlantic, the May zonal wind stress anomaly leads to thermocline changes that are most pronounced in June (Figure S3b). Also, these time series are highly correlated at 0.89 and 0.92, respectively. We find a slightly stronger thermocline slope response for a weakening ($10.60 \pm 2.34\,\mathrm{m/10^{-2}\,N\,m^{-2}}$) compared to a strengthening ($8.19 \pm 1.43\,\mathrm{m/10^{-2}\,N\,m^{-2}}$) of the trade winds (Figure 3c), but taking into account the error bounds, this difference is not significant. The difference is larger and significant in the Pacific, where the November–December thermocline slope response across the equatorial Pacific to the October–November western Pacific wind stress variations amounts to $12.91 \pm 1.13\,\mathrm{m/10^{-2}\,N\,m^{-2}}$ for a weakening but only $9.84 \pm 1.49\,\mathrm{m/10^{-2}\,N\,m^{-2}}$ for a strengthening of the winds (Figure 3d). This asymmetry

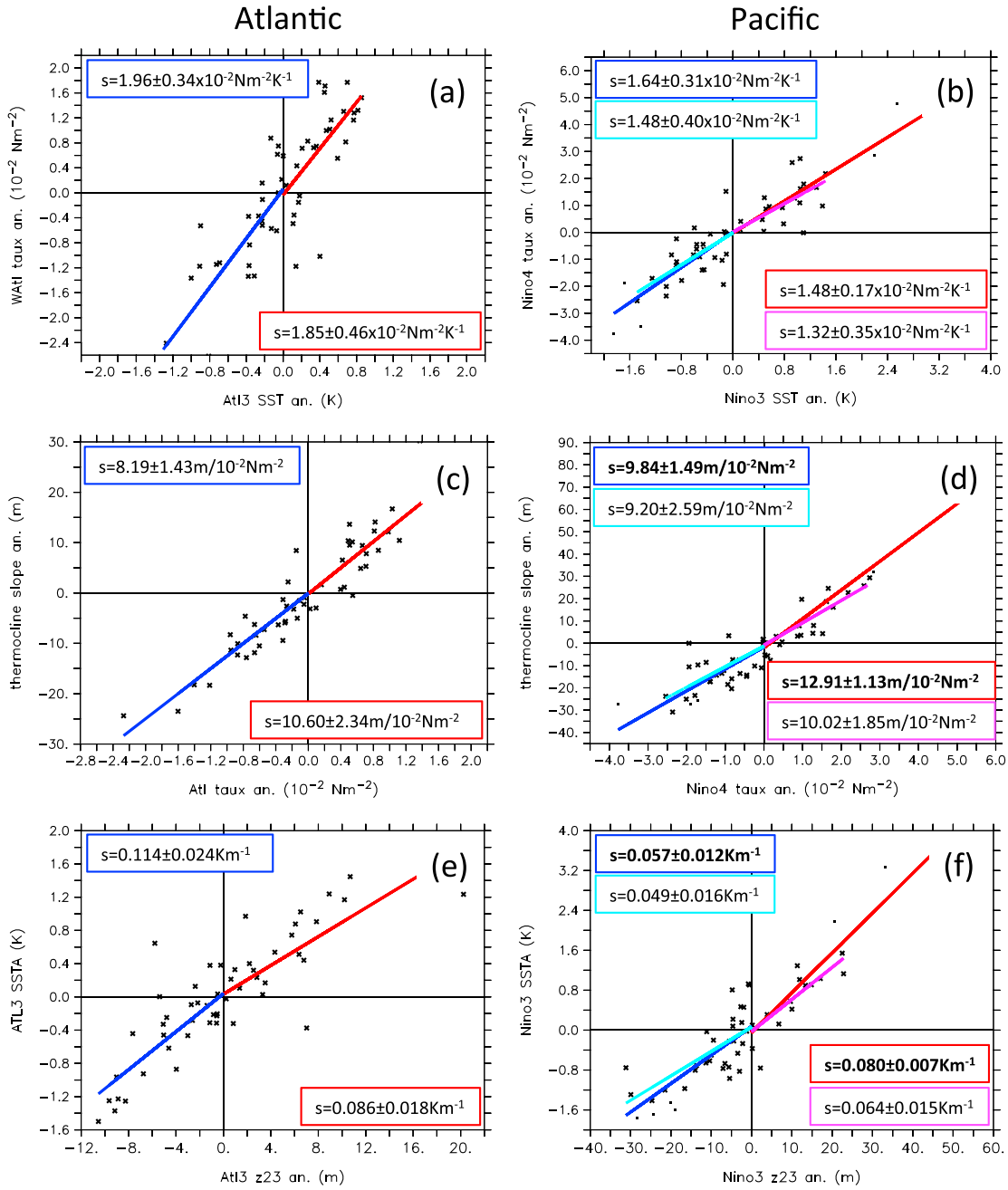

Figure 3. Bjerknes feedback components for (a, c, and e) equatorial Atlantic and (b, d, and f) equatorial Pacific: Linear regression between May Atl3 SST and May WAtl zonal wind stress anomalies (Figure 3a), October–November Nino3 SST and October–November Nino4 zonal wind stress anomalies (Figure 3b), May WAtl zonal wind stress and June Atlantic equatorial thermocline slope anomalies (Figure 3c), October–November Nino4 zonal wind stress and November–December Pacific equatorial thermocline slope anomalies (Figure 3d), June Atl3 thermocline depth and June Atl3 SST anomalies (Figure 3e), November–December Nino3 thermocline depth and December–January Nino3 SST anomalies (Figure 3f). Thermocline depth is defined as the depth of the 23°C isotherm, designated z23. In the Pacific panels, the red and blue lines show the regression slopes from all data points (dots) while for the magenta and light blue lines the range of Nino3 SST anomalies has been limited to the ones of Atl3 SST anomalies (crosses). The numbers refer to the regression slopes (s) with 95% error bounds. Bold font indicates that the regression slopes are significantly different from one another.

is in good agreement with the difference in the Bjerknes index parameter β_h that *Im et al.* [2015] found between El Niño and La Niña phases. Interestingly, we find only an insignificant difference between the Pacific and Atlantic, in contrast to *Lübbecke and McPhaden* [2013]. This is due to the fact that in the previous study all calendar months were considered and that a strong relationship between wind stress and

thermocline slope exists for almost all of the year in the equatorial Pacific while it is restricted to boreal spring and summer in the equatorial Atlantic (Figures S3b and S4b).

The third feedback component, i.e., the relation between an eastern basin thermocline depth anomaly and SSTs, is strongly asymmetric in the Pacific. In general, this subsurface-surface coupling works via upwelling and is strongest at a lag of about a month (Figures S3c and S4c). While a deepening of the thermocline in November–December is associated with a warming of $0.080 \pm 0.007\,\mathrm{K\,m^{-1}}$ in December–January, the corresponding shoaling of the thermocline is associated with a cooling of only $0.057 \pm 0.012\,\mathrm{K\,m^{-1}}$ (Figure 3f); i.e., the subsurface-surface coupling is significantly stronger for warm compared to cold events. This is in agreement with *Meinen and McPhaden* [2000, their Figure 7] who found a bigger SST response for a WWV increase than for a decrease. In contrast, the feedback is more symmetric in the Atlantic and even slightly stronger for cold events, though the difference is within the error bounds (Figure 3e). A deepening of the thermocline in June is associated with a warming of $0.086 \pm 0.018\,\mathrm{K\,m^{-1}}$, while a shoaling of the thermocline is associated with a cooling of $0.114 \pm 0.024\,\mathrm{K\,m^{-1}}$. As for the first two feedback components, we notice that the strength of the thermocline depth-SST relationship in the Atlantic is as strong or even stronger than for the Pacific, in contrast to the thermocline feedback calculated for all calendar months [*Lübbecke and McPhaden*, 2013], which highlights the more pronounced seasonality in the equatorial Atlantic.

To summarize, all components of the Bjerknes feedback are found to be essentially symmetric for the warm and cold phases of the Atlantic Niño mode. In contrast, in the Pacific, both the thermocline slope response to western basin zonal wind stress anomalies and the SST response to thermocline depth anomalies appear to be stronger for the warm phase of ENSO. To check whether these findings are sensitive to the ocean reanalysis product, we have repeated the analysis using SODA2.2.4 for the same time period (Figure S5). While the individual values show some differences, especially for the Atlantic Ocean where the correlations are lower and the uncertainties are higher, the main results are robust: The SST response to thermocline depth changes is stronger for a deepening than for a shoaling of the thermocline in the eastern equatorial Pacific, while none of the feedback components for the equatorial Atlantic shows a significant difference between warm and cold phases.

To investigate whether the Atlantic Niño mode is more symmetric than ENSO because of the overall smaller amplitude of the SST anomalies, we have repeated the regression analysis for the Pacific with Nino3 SST anomalies limited to the range of Atl3 SST anomalies (−1.50 to +1.68°C). The regression slopes for warm and cold phases are indeed more symmetric when the amplitude range is limited (magenta and light blue lines in Figure 3). This is the case for all three feedbacks and regardless whether all calendar months or only certain months are considered.

3.3. Heat Flux Damping for Warm and Cold Events

SST anomalies are damped by the net surface heat flux; i.e., heat is released from the ocean to the atmosphere during a warm event and taken up by the ocean during a cold event. *Nnamchi et al.* [2015] have suggested that heat fluxes might also play a role in forcing Atlantic Niño events, but once an SST anomaly has developed, heat fluxes certainly act as a damping. Interestingly, we find that the thermal damping, calculated as the regression between eastern basin SST and net surface heat flux anomalies, is more symmetric for warm and cold anomalies in the Pacific than in the Atlantic. In the Atlantic, the thermal damping for May-June-July amounts to $\alpha = -23.0 \pm 4.5\,\mathrm{W\,m^{-2}\,K^{-1}}$ for warm Atl3 SST anomalies and $\alpha = -15.9 \pm 6.0\,\mathrm{W\,m^{-2}\,K^{-1}}$ for cold anomalies, suggesting a stronger damping of Atlantic Niño events. The heat flux terms have, however, large uncertainties as evident in the large error bounds for the thermal damping. The difference might thus not be significant. In the Pacific on the other hand, the estimates for November-December-January is found to be almost the same for warm and cold phases ($-16.2 \pm 1.7\,\mathrm{W\,m^{-2}\,K^{-1}}$ for warm and $-16.1 \pm 4.4\,\mathrm{W\,m^{-2}\,K^{-1}}$ for cold Nino3 SST anomalies). This symmetry of the thermal damping is in disagreement with the results by *Im et al.* [2015] who found stronger thermal damping for El Niño compared to La Niña events, but again, the rather large error bounds, especially for the cold phases, need to be taken into consideration. There might also be some compensation between different terms, e.g., the latent heat and the shortwave feedback that tends to be poorly represented in models [e.g., *Bellenger et al.*, 2014].

4. Summary and Discussion

Using two different reanalysis products (ORA-S4 and SODA2.2.4), we show that the Atlantic Niño mode is much more symmetric than ENSO in the Pacific with respect to amplitude, location, and temporal evolution of warm and cold events. As shown by a composite analysis (Figures 1 and 2) Atlantic Niños and Niñas are essentially mirror images of each other, with maximum anomalies reaching similar amplitudes at the same location during the same months of the year. As for the symmetry in amplitude, a regression analysis performed separately for warm and cold anomalies suggests that it can be explained by the symmetric strength of the Bjerknes feedbacks, in contrast to the Pacific, where the responses are stronger for El Niño events (Figure 3).

It is interesting to note that in contrast to some previous studies that have highlighted the importance of nonlinearities in the SST-wind stress feedback for the asymmetry of ENSO, we find that the relation between variations in thermocline depth and SST in the eastern equatorial Pacific plays a dominant role. This asymmetry in the subsurface-surface coupling is consistent with the results of *Meinen and McPhaden* [2000] and also with the importance of ocean dynamics in accounting for the differences between El Niño and La Niña amplitudes as shown by *Im et al.* [2015]. The implications of these findings should be investigated in more detail in future studies.

Our analysis of Bjerknes feedback components, as summarized in Figure 3, supports not only our conclusion that Atlantic Niños are more symmetric than ENSO in the Pacific but also the hypothesis itself that the Bjerknes feedback is operative in the Atlantic given the strength of the relationship between the key variables involved in this mechanism. This does, however, not exclude the possibility that other processes such as heat flux forcing or meridional advection may be important in the generation of individual warm and cold events. Also, while we find that Atlantic warm and cold events appear as the inverse of one another, asymmetries might still exist in the forcing of Atlantic Niños and Niñas. For example, *Lübbecke et al.* [2014] showed that for those events that are affected by the strength of the South Atlantic Anticyclone (SAA), anomalies of the SAA in different months are important for the development of warm and cold SST anomalies. *Burmeister et al.* [2016] also suggested that meridional advection of temperature anomalies might play a larger role for warm than for cold events.

By repeating the regression analysis for the Pacific with Nino3 SST anomalies limited to the range of Atl3 SST anomalies, we have shown that the comparatively symmetric behavior of the Atlantic Niño mode is related to the overall smaller amplitude of the SST anomalies, which is in part a result of the smaller basin size [*Zebiak*, 1993; *Lübbecke and McPhaden*, 2013]. Furthermore, SST variability associated with the Atlantic Niño mode is much more closely linked to the seasonal cycle of SST than it is the case in the tropical Pacific, as shown, for example, by *Burls et al.* [2012]. They demonstrated that while in the Pacific interannual and seasonal variability are clearly distinct, interannual variability in the Atlantic can be understood as a modulation of the seasonally active thermocline mode. In this framework, Atlantic warm and cold events are generated by variations in the timing and intensity of seasonal cold tongue development. These perturbations might be fairly symmetrically distributed, i.e., an amplification of the seasonal cycle is as likely as suppression, and an early onset of the cold tongue occurs as often as a late onset.

Acknowledgments
We thank three anonymous reviewers for their thoughtful comments on an earlier version of this manuscript. This study is a contribution of the SFB 754 supported by the Deutsche Forschungsgemeinschaft. Both reanalysis products (SODA2.2.4 and ECMWF ORA-S4) are provided by the Integrated Climate Data Center at http://icdc.zmaw.de/projekte/easy-init/easy-init-ocean. All of the SST data sets used for Table S1 are available from www.esrl.noaa.gov/psd/data/gridded/tables/sst.html. PMEL contribution 4512.

References

Balmaseda, M. A., K. Mogensen, and A. T. Weaver (2013), Evaluation of the ECMWF Ocean Reanalysis System ORA-S4, *Q. J. R. Meteorol. Soc.*, *139*, 1132–1161, doi:10.1002/qj.2063.

Bellenger, H., E. Guilyardi, J. LeLoup, M. Lengaigne, and J. Vialard (2014), ENSO representation in climate models: From CMIP3 to CMIP5, *Clim. Dyn.*, *42*, 1999–2018, doi:10.1007/s00382-013-1783-z.

Bjerknes, J. (1969), Atmospheric teleconnections from the equatorial Pacific, *Mon. Weather Rev.*, *97*, 163–172.

Brandt, P., G. Caniaux, B. Boulès, A. Lazar, M. Dengler, A. Funk, V. Hormann, H. Giordani, and F. Marin (2011a), Equatorial upper-ocean dynamics and their interaction with the West African monsoon, *Atmos. Sci. Lett.*, *12*, 24–30, doi:10.1002/asl.287.

Brandt, P., A. Funk, V. Hormann, M. Dengler, R. J. Greatbatch, and J. M. Toole (2011b), Interannual atmospheric variability forced by the deep equatorial Atlantic Ocean, *Nature*, *473*, 497–501, doi:10.1038/nature10013.

Burls, N. J., C. J. Reason, P. Penven, and S. G. Philander (2012), Energetics of the tropical Atlantic zonal mode, *J. Clim.*, *25*, 7442–7466, doi:10.1175/JCLI-D-11-00602.1.

Burmeister, K., P. Brandt, and J. F. Lübbecke (2016), Revisiting the cause of the eastern equatorial cold event in 2009, *J. Geophys. Res. Oceans*, *121*, 4777–4789, doi:10.1002/2016JC011719.

Carton, J., and B. S. Giese (2008), A reanalysis of ocean climate using Simple Ocean Data Assimilation (SODA), *Mon. Weather Rev.*, *136*, 2999–3017, doi:10.1175/2007MWR1978.1.

Carton, J., and B. Huang (1994), Warm events in the tropical Atlantic, *J. Phys. Oceanogr.*, *24*, 888–903.

Chang, P., et al. (2006), Climate fluctuations of tropical coupled systems—The role of ocean dynamics, *J. Clim.*, *19*, 5122–5271.
Choi, K.-Y., G. A. Vecchi, and A. T. Wittenberg (2013), ENSO transition, duration, and amplitude asymmetries: Role of the nonlinear wind stress coupling in a conceptual model, *J. Clim.*, *26*, 9462–9467, doi:10.1175/JCLI-D-13-00045.1.
Compo, G. P., et al. (2011), The twentieth century reanalysis project, *Q. J. R. Meteorol. Soc.*, *137*, 1–28, doi:10.1002/qj.776.
Deppenmeier, A.-L., R. J. Haarsma, and W. Hazeleger (2016), The Bjerknes feedback in the tropical Atlantic in CMIP5 models, *Clim. Dyn.*, doi:10.1007/s00382-016-2992-z.
Dommenget, D., T. Bayr, and C. Frauen (2012), Analysis of the non-linearity in the pattern and time evolution of El Niño southern oscillation, *Clim. Dyn.*, doi:10.1007/s00382-012-1475-0.
Frauen, C., and D. Dommenget (2010), El Niño and La Niña amplitude asymmetry caused by atmospheric feedbacks, *Geophys. Res. Lett.*, *37*, L18801, doi:10.1029/2010GL044444.
Hoerling, M. P., A. Kumar, and M. Zhong (1997), El Nino, La Nina, and the nonlinearity of their teleconnection, *J. Clim.*, *10*, 1769–1786.
Hu, Z.-Z., and B. Huang (2007), Physical processes associated with tropical Atlantic SST gradient during the anomalous evolution in the southeastern ocean, *J. Clim.*, *20*, 3366–3378, doi:10.1175/JCLI4189.1.
Im, S.-H., S.-I. An, S. T. Kim, and F.-F. Jin (2015), Feedback processes responsible for El Niño-La Niña amplitude asymmetry, *Geophys. Res. Lett.*, *42*, 5556–5563, doi:10.1002/2015GL064853.
Jin, F.-F., S. T. Kim, and L. Bejarano (2006), A coupled-stability index for ENSO, *Geophys. Res. Lett.*, *33*, L23708, doi:10.1029/2006GL027221.
Kang, I.-S., and J.-S. Kug (2002), El Niño and La Niña sea surface temperature anomalies: Asymmetry characteristics associated with their wind stress anomalies, *J. Geophys. Res.*, *107*(D19), 4372, doi:10.1029/2001JD000393.
Keenlyside, N. S., and M. Latif (2007), Understanding equatorial Atlantic interannual variability, *J. Clim.*, *20*, 131–142, doi:10.1175/JCLI3992.1.
Keenlyside, N. S., H. Ding, and M. Latif (2013), Potential of equatorial Atlantic variability to enhance El Niño prediction, *Geophys. Res. Lett.*, *40*, 2278–2283, doi:10.1002/grl.50362.
Larkin, N. K., and D. E. Harrison (2002), ENSO warm (El Nino) and cold (La Nina) event life cycles: Ocean surface anomaly patterns, their symmetries, asymmetries, and implications, *J. Clim.*, *15*, 1118–1140.
Lübbecke, J. F., and M. J. McPhaden (2013), A comparative stability analysis of Atlantic and Pacific Niño modes, *J. Clim.*, *26*, 5965–5980, doi:10.1175/JCLI-D-12-00758.1.
Lübbecke, J. F., C. W. Böning, N. S. Keenlyside, and S.-P. Xie (2010), On the connection between Benguela and equatorial Atlantic Niños and the role of the South Atlantic Anticyclone, *J. Geophys. Res.*, *115*, C09015, doi:10.1029/2009JC005964.
Lübbecke, J. F., N. J. Burls, C. J. C. Reason, and M. J. McPhaden (2014), Variability in the South Atlantic Anticyclone and the Atlantic Niño Mode, *J. Clim.*, *27*, 8135–8150, doi:10.1175/JCLI-D-14-00202.1.
Meinen, C. S., and M. J. McPhaden (2000), Observations of warm water volume changes in the equatorial Pacific and their relationship to El Niño and La Niña, *J. Clim.*, *13*, 3551–3559.
Nnamchi, H. C., J. Li, F. Kucharski, I.-S. Kang, N. S. Keenlyside, P. Chang, and R. Farneti (2015), Thermodynamic controls of the Atlantic Niño, *Nat. Commun.*, *6*, 8895, doi:10.1038/ncomms9895.
Richter, I., S. K. Behera, Y. Masumoto, B. Taguchi, H. Sasaki, and T. Yamagata (2013), Multiple causes of interannual sea surface temperature variability in the equatorial Atlantic Ocean, *Nat. Geosci.*, *6*(1), 43–47, doi:10.1038/ngeo1660.
Rodriguez-Fonseca, B., I. Polo, J. Garcia-Serrana, T. Losada, E. Mohino, C. R. Mechoso, and F. Kucharski (2009), Are Atlantic Niños enhancing Pacific ENSO events in recent decades?, *Geophys. Res. Lett.*, *36*, L20705, doi:10.1029/2009GL040048.
Ruiz-Barradas, A., J. A. Carton, and S. Nigam (2000), Structure of interannual-to-decadal climate variability in the tropical Atlantic sector, *J. Clim.*, *13*, 3285–3297.
Shinoda, T., H. E. Hurlburt, and E. J. Metzger (2011), Anomalous tropical ocean circulation associated with La Niña Modoki, *J. Geophys. Res.*, *116*, C12001, doi:10.1029/2011JC007304.
Su, J., R. Zhang, T. Li, X. Rong, J. S. Ug, and C. C. Hong (2010), Causes of the El Niño and La Niña amplitude asymmetry in the equatorial eastern Pacific, *J. Clim.*, *23*, 605–617, doi:10.1175/2009JCLI2894.1.
Zebiak, S. E. (1993), Air-sea interaction in the equatorial Atlantic region, *J. Clim.*, *6*, 1567–1586.